

4-2015

An Integrated 700–1200 MHz Class-F PA with Tunable Harmonic Terminations in 0.13 μ m CMOS

Kossi K. Sessou
Iowa State University

Nathan M. Neihart
Iowa State University, neihart@iastate.edu

Follow this and additional works at: https://lib.dr.iastate.edu/ece_pubs



Part of the [Electrical and Computer Engineering Commons](#)

The complete bibliographic information for this item can be found at https://lib.dr.iastate.edu/ece_pubs/235. For information on how to cite this item, please visit <http://lib.dr.iastate.edu/howtocite.html>.

This Article is brought to you for free and open access by the Electrical and Computer Engineering at Iowa State University Digital Repository. It has been accepted for inclusion in Electrical and Computer Engineering Publications by an authorized administrator of Iowa State University Digital Repository. For more information, please contact digirep@iastate.edu.

An Integrated 700–1200 MHz Class-F PA with Tunable Harmonic Terminations in 0.13 μ m CMOS

Abstract

A fully integrated class-F power amplifier (PA) with reconfigurable harmonic termination over a wide range of frequencies is presented. Reconfigurability is achieved by utilizing on-chip transformers as part of the output matching network. In addition, a stacked transistor architecture was used to boost the output power. The PA was fabricated in a 0.13- μ m CMOS process and packaged in a 20-pin quad flat no-leads package. It was configured to operate at 700, 900, and 1200 MHz with a maximum measured saturated output power of +24.6 dBm with a power-added efficiency of 48.3%. The measured gain was 16.5 dB and was flat over the entire bandwidth. The total chip area, including pads, is 1.5 mm \times 1.5 mm.

Keywords

Power amplifiers, reconfigurable matching network

Disciplines

Electrical and Computer Engineering

Comments

This is a manuscript of an article published as Sessou, Kossi K., and Nathan M. Neihart. "An Integrated 700–1200 MHz Class-F PA with Tunable Harmonic Terminations in 0.13 μ m CMOS." *IEEE Transactions on Microwave Theory and Techniques* 63, no. 4 (2015): 1315-1323. DOI: [10.1109/TMTT.2015.2403843](https://doi.org/10.1109/TMTT.2015.2403843).
Posted with permission.

An Integrated 700–1200 MHz Class-F PA with Tunable Harmonic Terminations in 0.13 μ m CMOS

Kossi K. Sessou, *Student Member, IEEE*, and Nathan M. Neihart, *Senior Member, IEEE*

Abstract—A fully integrated class-F power amplifier with reconfigurable harmonic termination over a wide range of frequencies is presented. Reconfigurability is achieved by utilizing an on-chip transformers as part of the output matching network. In addition, a stacked transistor architecture was used to boost the output power. The power amplifier was fabricated in a 0.13 μ m CMOS process and packaged in a 20-pin quad flat no-leads (QFN) package. It was configured to operate at 700 MHz, 900 MHz, and 1200 MHz with a maximum measured saturated output power of +24.6 dBm with a power added efficiency of 48.3%. The measured gain was 16.5 dB and was flat over the entire bandwidth. The total chip area, including pads, is 1.5 mm \times 1.5 mm.

Index Terms—Power amplifiers, reconfigurable matching network

I. INTRODUCTION

MAINTAINING high efficiency and good linearity across multiple different frequency bands, modulation standards, and bandwidths are fundamental challenges for next generation power amplifier (PA) designers. With wireless technology becoming almost ubiquitous and with the types of enriched and enhanced features and services that are provided to the end user, mobile devices are in high demand to support higher data rates [1]–[5]. As a consequence, there is independent development of several spectrally efficient communication standards such as long-term evolution (LTE) and worldwide interoperability for microwave access (WiMAX), which is increasing the number of frequency bands and the amount of spectrum fragmentation [6]. This is creating an environment wherein wireless systems must communicate over many different, sometimes non-adjacent, frequency bands. Furthermore, to facilitate network migration and permit wide geographic roaming, systems must also support multiple legacy-standards as well, further complicating the problem.

In order to provide the required level of support, current transmitters utilize multiple, parallel PAs, with each separate PA dedicated to a specific communication standard and/or band within a given standard. As a result, large, complex, and expensive PA modules are inevitable. In an effort to address this issue, researchers have recently begun to develop frequency agile PAs capable of covering several frequency bands [3], [7]–

[9]. Several common techniques for increasing the versatility of PAs exist: using a single power cell bundled with many, parallel matching networks and switches [7]; using reconfigurable matching networks [8]; and using broadband PAs that simultaneously cover all desired frequency bands [3], [9].

Using a single power cell with multiple switched matching networks, is not much more area efficient than using multiple, parallel power amplifiers. The size of the passive matching network, which typically will not scale with technology, can easily rival the size of the power cell. Another, potentially more serious issue with switchable matching networks is the insertion loss of the switches which directly reduces efficiency. The area of the matching network can be reduced by using a reconfigurable matching network, where the usage of tunable elements, most notably varactors [8], can allow the tuning of a single matching network over a wide range of frequencies. Using tunable elements in the signal path, however, can result in serious non-linear distortion.

Another approach is to use broadband PAs in order to cover multiple bands simultaneously. A very common method to achieving wideband operation is to use a distributed architecture [10]. Unfortunately, distributed PAs suffer from large area and relatively low efficiencies. An alternative is to use a broadband output matching network [9], but these are not compatible with some currently popular high-efficiency PA architectures.

In this paper, we present a fully integrated CMOS class-F PA capable of reconfigurable operation from 700 MHz to 1200 MHz. Other high-efficiency switch-mode/harmonic-tuned PA topologies exist, such as class-D, E, and J, but due to the limited device speed, class-D topologies are of limited use at microwave frequencies. Class-E PA topologies also have device speed limitations as well as drain voltages as large as 3.6 times the supply voltage, making class-E difficult to realize in low-breakdown technologies such as CMOS. Class-F on the other hand, has a maximum drain voltage that is only 2 times higher than the supply and therefore more amenable for CMOS implementation [11]–[14].

The bandwidth of a class-F PA is limited in practice by the requirement to precisely terminate the 2nd and 3rd harmonics at the output. One way to increase the bandwidth is to use a class-

J topology which requires a reactive component at the fundamental to maintain the second harmonic phasing thereby boosting efficiency [15]. Class-J becomes overly complex, however, and is not well suited for the type of load tuning we are proposing. The proposed system gets around this issue by using a novel reconfigurable output matching network capable of providing real-time tuning of the 2nd and 3rd harmonic terminations to support a fundamental frequency range of 700–1200 MHz. High efficiency over the entire range of frequencies is thereby maintained. This reconfigurability is achieved through the use of integrated transformers [16–18] and a bank of parallel capacitors. It is important to realize that this PA is not intended for signals with instantaneous bandwidths of 500 MHz, instead it supports narrow-band signals over a wide range of potential carrier frequencies. Moreover, all techniques presented can be easily adapted to a class-F⁻¹ topology.

This paper is organized as follows, in Section II, the design theory of the proposed PA is presented and the reconfigurable output matching network is explained. The circuit implementation is discussed in Section III. In Section IV experimental results are presented, and finally, the paper concludes in Section V.

II. DESIGN OF A TRANSFORMER-BASED RECONFIGURABLE POWER AMPLIFIER

A. Traditional Class-F Operation

An ideal class-F power amplifier can achieve a theoretical drain efficiency of 100% by using harmonic resonators in the output matching network to shape the drain-voltage and drain-current waveforms. A maximized efficiency is achieved when the drain-voltage is a square wave and the drain-current is a half-rectified sine wave and this condition is achieved by presenting a short-circuit to all even-order harmonics and an open-circuit to all odd-order harmonics. Table I shows how the efficiency changes with varying levels of harmonic control [19]. In practice, controlling harmonics beyond the 3rd harmonic results in a significant increase in complexity with only marginal improvements in the overall efficiency [4], so many practical designs only control the 2nd harmonic of the drain current and the 3rd harmonic of the drain voltage which, from Table I, results in a theoretical maximum drain efficiency of 75%.

B. Transformer Based Output Network

In typical class-F operation, resonators (both lumped and distributed) are used for harmonic peaking at fixed frequencies thereby limiting the overall bandwidth of the PA. At the heart of the proposed tunable class-F load is a high-order transformer-based resonator, shown in Fig. 1(a), that allows the user to control the frequency at which the load presents a short-circuit (e.g., for terminating the 2nd harmonic) and an open-circuit (e.g., for terminating the 3rd harmonic). A simple analysis of the resonator shows that the input impedance of the network is:

$$Z_{IN}(s) = sL_1 - \frac{s^2 M^2}{sL_2 + 1/sC_2} + Z_{LOAD}(s) \quad (3)$$

where $M = k\sqrt{L_1 L_2}$ is the mutual inductance between

TABLE I. CLASS-F EFFICIENCY AS A FUNCTION OF VOLTAGE AND CURRENT HARMONIC CONTENT

Current Harmonic Comp.	Voltage Harmonic Component		
	1	1,3	1,3,5,...,∞
1	0.500	0.563	0.637
1,2	0.667	0.750	0.849
1,2,4,...,∞	0.785	0.884	1.000

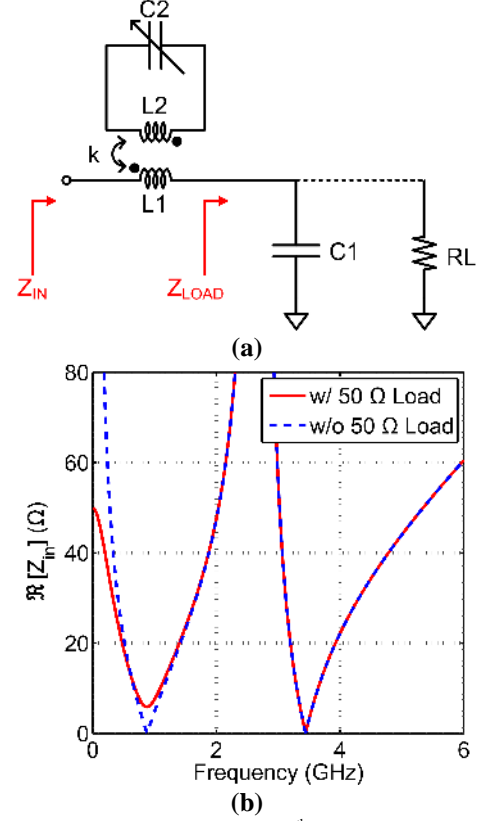


Fig. 1. (a) Schematic of the proposed 4th-order resonant tank and (b) frequency response of Z_{IN} with real and complex load.

inductors L_1 and L_2 with coupling coefficient k . In order to simplify the analysis and gain some insight we begin by assuming that the load impedance is purely capacitive and $Z_{LOAD} = 1/sC_1$. The input impedance can now be written as:

$$Z_{IN}(s) = \frac{s^4(L_1 C_1 C_2 - k^2 C_1 C_2 L_1^2) + s^2(C_1 + C_2)L_1 + 1}{s C_1 (s^2 L_2 C_2 + 1)}. \quad (4)$$

Under these assumptions, it can be shown that Z_{IN} has a pole at dc and a pair of complex conjugate poles located at:

$$f_{p2,3} = \pm \frac{1}{2\pi} \sqrt{\frac{1}{L_2 C_2}} \quad (5)$$

and two real zeroes located at:

$$f_{z1} = \frac{f_1^2 + f_2^2 - \sqrt{f_1^4 + f_2^4 + f_1^2 f_2^2 (4k^2 - 2)}}{2(1 - k^2)} \quad (6)$$

$$f_{z2} = \frac{f_1^2 + f_2^2 + \sqrt{f_1^4 + f_2^4 + f_1^2 f_2^2 (4k^2 - 2)}}{2(1 - k^2)} \quad (7)$$

where $f_1 = 1/(2\pi\sqrt{L_1 C_1})$ and $f_2 = 1/(2\pi\sqrt{L_2 C_2})$.

We aim to control the location of the poles and zeroes given the five parameters L_1 , C_1 , L_2 , C_2 , and k . From this point forward, we will consider our system as having two distinct zeroes located at f_{z1} and f_{z2} and a pole located at $f_{p2,3}$ because

the complex poles will have the same real part. It can be shown from (4)–(7) that only two of the three poles/zeros can be independently controlled. In the realm of class-F PA design, we would like to place the low-frequency zero, f_{z1} , at the fundamental. A high-impedance open circuit can then be placed at the 3rd harmonic by setting the complex conjugate poles, $f_{p2,3}$, appropriately. The high frequency zero, f_{z2} , will then fall outside of the band of interest.

In the above analysis, Z_{LOAD} was assumed to be purely capacitive. When a resistor, R_L , is added in parallel with C_1 , the expression for the input impedance becomes as shown in (8). Notice that the location of the poles $f_{p2,3}$ and the zeros $f_{z1,2}$ have not changed. The DC pole, however, has been shifted and is now located at $f_{p1} = 1/(2\pi R_L C_1)$. This will cause a slight change in the reactance of Z_{IN} at low frequencies (outside of the band of interest). What is perhaps not as obvious is the fact that the load network in Fig. 1(a) can be used as an impedance transformation network in the low-band where the transformation ratio is controlled by the values of L_1 and C_1 .

As an example, consider a class-F PA operating at 900 MHz. We wish to pass the fundamental frequency by setting $f_{z1} = 900$ MHz while providing a high-impedance to the 3rd harmonic by setting $f_{p2,3} = 2700$ MHz (in this example we are neglecting the short-circuit presented at the 2nd harmonic which can be achieved by including an additional transformer network). Such a network can be realized using $L_1 = 4$ nH, $L_2 = 2.4$ nH, $k = 0.6$, $C_1 = 7.5$ pF, and $C_2 = 1.4$ pF. The input impedance for this example is plotted in Fig. 1(b) for two cases: when Z_{LOAD} is purely capacitive and when Z_{LOAD} is complex. As expected the network presents a low impedance at 900 MHz and a very high impedance at 2700 MHz. Also notice that the load network has transformed the 50 Ω load down to approximately 5 Ω . Moreover, the high-frequency zero, f_{z2} , is located at 3450 MHz, well beyond the band of interest.

As previously mentioned, the locations for f_{z1} , f_{z2} , and $f_{p2,3}$ cannot all be set independently and it is seen in (5)–(7) that they all depend upon the values of f_1 and f_2 . Graphical visualization is the best way to determine the values of f_1 and f_2 that realize a given desired location of the poles and zeroes. Fig. 2 shows the contours for three different pairs of f_{z1} and $f_{p2,3}$ plotted against f_1 and f_2 with the added condition that $f_{p2,3} = 3f_{z1}$. The points where the contours intersect represent values of f_1 and f_2 that are valid solutions for (5) and (6). To see where the high-frequency zero, f_{z2} , is located, (7) is also plotted in Fig. 2. Doing so shows that there is a unique contour for f_{z2} that passes through each intersection of f_{z1} and $f_{p2,3}$. The different solutions are marked in Fig. 2 by S1, S2, and S3, for the fundamental frequencies of 700 MHz, 900 MHz, and 1200 MHz, respectively. In each case, the location of f_{z2} is located at frequencies higher than the 3rd harmonic.

Once the values of f_1 and f_2 have been determined, it becomes necessary to determine the component values for the

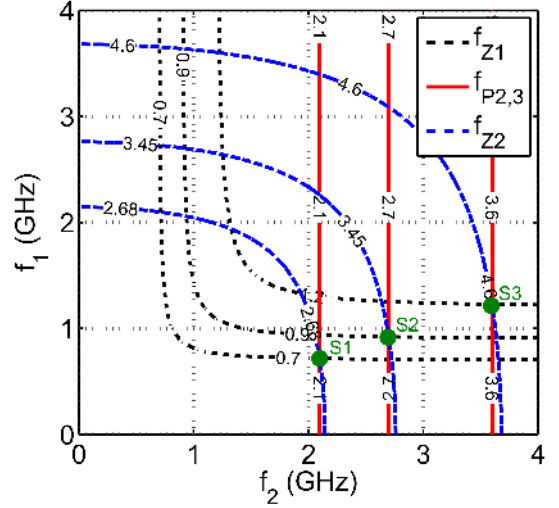


Fig. 2. Contour plot of f_{z1} , $f_{p2,3}$, and f_{z2} as functions of f_1 and f_2 . Points S1, S2, and S3 indicate valid solutions of f_1 and f_2 for operation at 700 MHz, 900 MHz, and 1200 MHz, respectively.

matching network. At this point, however, there are an infinite number of solutions that satisfy a given set of values for f_1 and f_2 . The required impedance scaling, however, introduces an additional constraint that results in a set of unique values for L_1 , C_1 , L_2 , and C_2 assuming that the coupling coefficient, k , has been previously set. The coupling coefficient is typically going to be determined by manufacturability considerations and values between 0.4 and 0.8 are commonly seen in on-chip transformers.

It is necessary, however, to examine the sensitivity of the matching network to variation in the value of the coupling coefficient. The coupling coefficient of on-chip transformers can vary by as much as 20%. To examine the effects of variation in k , the curves in Fig. 2 are re-plotted keeping all values constant but with either a 10% decrease in k (Fig. 3(a)) or a 10% increase in k (Fig. 3(b)). It is seen that the location of the complex conjugate poles is insensitive to variations in the coupling coefficient, which is expected from (5). In addition, the low-frequency zero, f_{z1} , shows minimal sensitivity to k as is evidenced by the solutions of f_1 and f_2 for the three cases. The value for f_1/f_2 for points S1, S2, and S3 in Fig. 2 are 0.72/2.1, 0.92/2.7, and 1.23/3.6, respectively. When k is decreased by 10% these values become 0.71/2.1, 0.92/2.7, and 1.23/3.6 and when k is increased by 10% they become 0.72/2.1, 0.93/2.7, and 1.24/3.6. The high-frequency zero, f_{z2} , however, is significantly impacted by variations in the coupling coefficient. This is acceptable, however, because it still remains well above the 3rd harmonic in all cases.

C. Design of the Stacked-FET Active Device

Modern CMOS processes are not tolerant to high supply voltages due to the thin gate oxide and its associated low breakdown voltage. If the process-dictated supply voltage is used, a large impedance transformation ratio will be required and the associated loss in the output matching network will

$$Z_{IN}(s) = \frac{s^4 L_1 C_1 L_2 C_2 R_L (1-k^2) + s^3 L_2 C_2 L_1 (1-k^2) + s^2 R_L (L_1 C_1 + L_2 C_2) + s L_1 + 1}{(s C_1 R_L + 1)(s^2 L_2 C_2 + 1)} \quad (8)$$

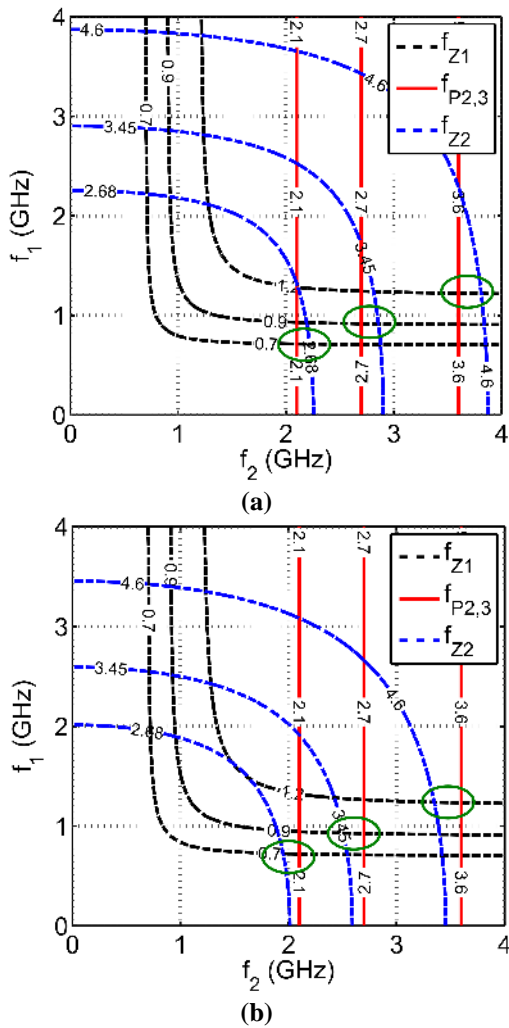


Fig. 3. Contour plots of f_{z1} , $f_{p2,3}$, and f_{z2} as functions of f_1 and f_2 showing variation when (a) k is decreased by 10% ($k = 0.54$) and (b) k is increased by 10% ($k = 0.66$).

reduce efficiency and output power. One way to alleviate this issue is to use a stacked-FET topology [1]. By stacking the transistors, the power cell can withstand a higher supply voltage resulting in an increased output power for a fixed load impedance. In general, the supply voltage can be scaled by a factor equal to the number of stacked transistors. Avalanche breakdown in the drain/bulk junction can occur, however, which places a fundamental limitation on the number of transistors that can be stacked.

III. CIRCUIT IMPLEMENTATION

The schematic of the proposed fully integrated class-F PA with reconfigurable harmonic termination is shown in Fig. 4 with component values given in Table II. By stacking transistors M1–M4, as shown in Fig. 4, the power cell can now withstand a supply voltage that is four times greater than that of a single transistor. The sizing of transistors M1–M4 is done iteratively with the aid of load pull simulations. All four devices are identically sized with a length of $0.12 \mu\text{m}$ and width of $2400 \mu\text{m}$ (divided across 140 fingers). The number of fingers is dictated by the peak drain current and is chosen such that the current density through each finger is kept under process

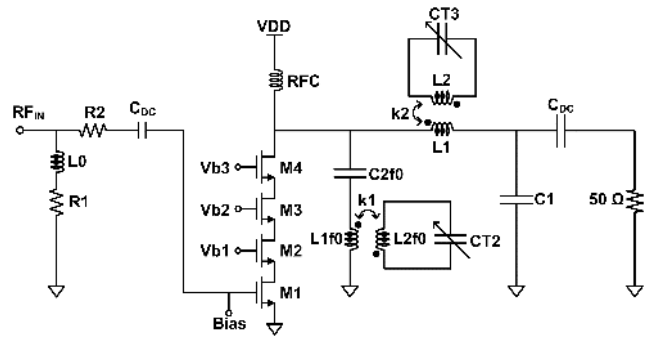


Fig. 4. Simplified schematic of the proposed class-F power amplifier with tunable harmonic termination.

TABLE II. COMPONENT VALUES FOR PROPOSED CLASS-F PA

Component	Value	Component	Value
R1	118.4 Ω	L2f0	2.1 nH
R2	98.7 Ω	C_{DC}	15 pF
L1	4.0 nH	C1	7.5 pF
L2	1.9 nH	C_{2f0}	1.99 pF
L1f0	1.74 nH	CT2	0.2 – 2 pF
L0	9.37 nH	RFC	9.37 nH
CT3	0.3–5.7 pF	k1/k2	0.52/0.65

TABLE III. LOAD PULL SIMULATION AT THE FREQUENCIES OF OPERATION

Freq. (MHz)	Load (Ω)	Max Power Added Efficiency (%)	Max Pout (dBm)
700	18.93 + j14.61	62.00	28.00
900	18.02 + j15.36	62.00	28.00
1200	17.62 + j15.76	62.00	28.00

maximums. In the targeted $0.13 \mu\text{m}$ CMOS process, the avalanche breakdown voltage of the drain/bulk junction is greater than 10 V and the oxide breakdown voltage is greater than 4.25 V. From simulation the maximum drain voltage of M4 is 9.75 V and the maximum voltage drop across any oxide is less than 4 V.

The reconfigurable output matching network is composed of two 4th-order resonators, which were described in Section II. The first resonator, consisting of L_1 , L_2 , C_1 , and C_{T3} controls the location of the 3rd-harmonic open-circuit termination as well as provides the necessary impedance transformation from 50Ω to the optimum load impedance as determined from load pull simulations shown in Table III. Since we cannot dynamically control the real part of Z_{IN} , we design the load network to provide the optimum match at 900 MHz knowing that the optimum termination at 700 and 1200 MHz will be close, but not exact, as seen in Table III.

The second resonator, consisting of L_{1f0} , L_{2f0} , C_{2f0} , and C_{T2} , controls the location of the 2nd-harmonic short-circuit termination. The frequency-location of the open- and short-circuit termination can then be controlled via variable capacitors, C_{T3} and C_{T2} , which are realized using a bank of fixed capacitors and switches. All of the switches are identically sized for minimum on-resistance with $W = 750.21 \mu\text{m}$ (divided into 51 fingers) and $L = 150 \text{ nm}$.

Using switches at this point in the load network does not

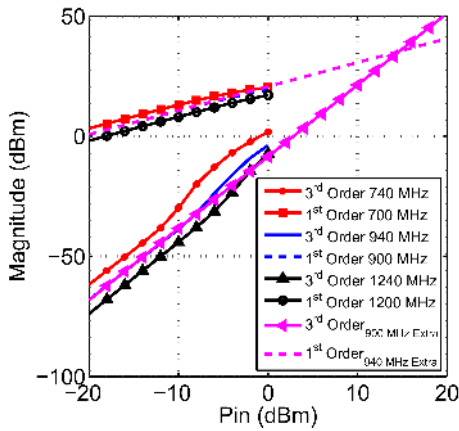


Fig. 5. Simulated OIP3 at 700, 900, and 1200 MHz.

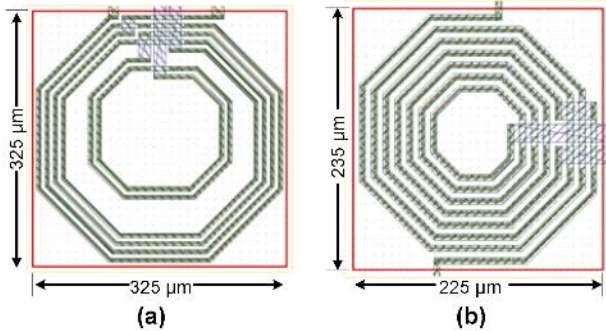


Fig. 6. Layout for the transformer used for (a) controlling the 3rd harmonic and (b) controlling the 2nd harmonic.

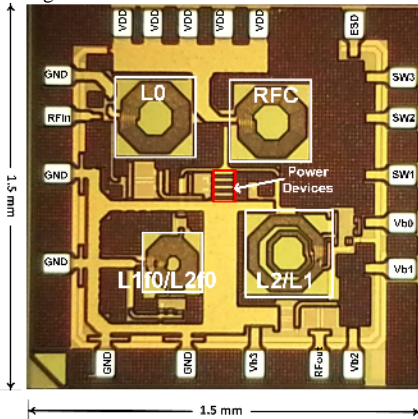


Fig. 7. Die microphotograph.

significantly impact the overall performance of the PA because they are partially isolated from the primary RF signal path by the coupling coefficient of the transformers. In addition, the transformer keeps the maximum voltage drop across the capacitor/switch pairs from becoming too large. Simulation results show that the maximum voltage drop across the switch/capacitor combination is only 7.2 V (despite the 9.75 V signal swing at the drain of M4) which is below the process defined maximum which is greater than 7.5 V.

Any time a tunable element is introduced, there is a potential impact on linearity. The linearity of the PA was evaluated using a two-tone simulation with 20 MHz tone spacing. As shown in Fig. 5 the simulated OIP3 is +35.46, +34.89 and +33.07 dBm at 700, 900, and 1200 MHz, respectively. All intercept points can be seen to be within 0.5 dB of each other indicating no significant degradation of linearity due to the tunable matching

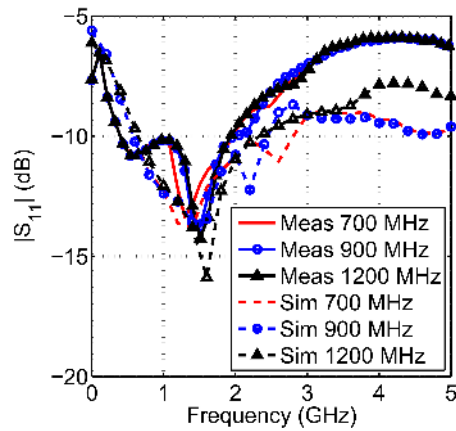


Fig. 8. Measured and simulated S11 for operation at 700, 900, and 1200 MHz.

network. This is because the capacitors are fixed-valued capacitors and switching does not occur during active transmission.

The transformers were designed and simulated using ADS Momentum and equivalent lumped-element models were created for use in both time-domain and frequency-domain simulations. A custom concentric transformer topology was used and the windings were realized as a parallel stack of the top two thick metal layers connected with a dense collection of vias. This will increase the quality factor of the windings and help to minimize the loss in the load network. The layout of the transformers used to control the 3rd-harmonic termination of the drain voltage and 2nd-harmonic termination of the drain current are shown in Fig. 6(a) and Fig. 6(b), respectively. The simulated loss of the matching network is -1.1, -1.5, and -2 dB at 700, 900, and 1200 MHz, respectively and is dominated by the relatively low-Q of the integrated inductors.

Finally, the input matching network consists of a resistive network with a wideband response as proposed in [20]. The value of R_1 is given by the series combination of R_2 and the parasitic gate resistance of M1, R_g . Resistor R_2 is primarily used for stabilization. The parasitic gate-source capacitance of M1, C_{gs} , and the value of R_1 are then used to determine the value of the inductor, L_0 , following guidelines found in [20].

IV. MEASUREMENT RESULTS

The proposed PA with real-time harmonic termination tuning capability was fabricated in a 0.13 μm CMOS process and occupies a total area of $1.5 \times 1.5 \text{ mm}^2$ including pads. The tunable matching network supports fundamental frequencies between 700 MHz and 1200 MHz. A die photo is shown in Fig. 7. For testing purposes, the die was packaged in a 20-pin quad flat no-leads (QFN) package and mounted to a double layer FR4 printed circuit board (PCB). All measurements are thus referred to the edge of the PCB.

Both small-signal and large-signal characterization was performed. An Agilent 5071C network analyzer was used to measure small-signal S-parameters. Measured S11 is compared to simulation in Fig. 8 when the PA is configured to operate at 700 MHz, 900 MHz, and 1200 MHz. The measured -10 dB bandwidth ranges from 400 MHz to 1800 MHz. The slight

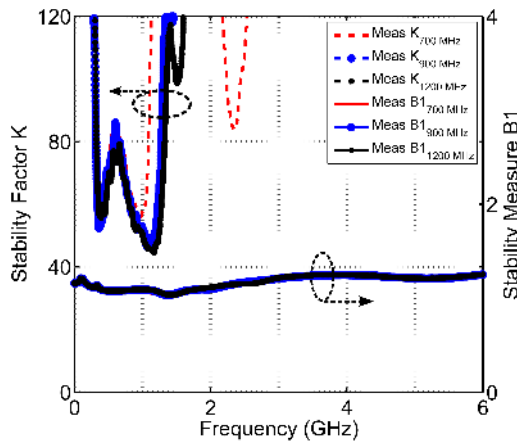


Fig. 9. Measured stability factor K and stability measure $B1$ for the proposed power amplifier.

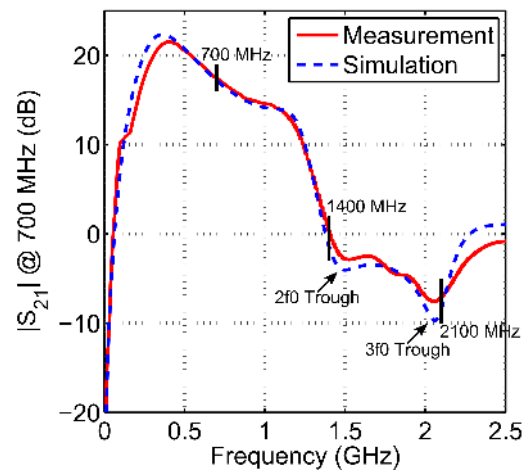
deviation from simulated results at high frequencies can be attributed to parasitics in the bond wires and PCB traces. The input impedance of the power amplifier at 700, 900, and 1200 MHz is $50.1 - j29.6 \Omega$, $43.3 - j29.6 \Omega$, and $36.4 - j20.9 \Omega$, respectively and the measured S_{22} is -2.4 , -3.5 , and -10.3 dB, respectively. Finally, we verified stability over the frequency range of 300 kHz to 6 GHz by plotting the Rollet stability factor, K , and stability measure, $B1$ in Fig. 9 [21]. As seen in Fig. 9, $K > 1$ and $B1 > 0$ for all frequencies thereby confirming stability.

Simulated and measured values for S_{21} are shown in Fig. 10(a) for 700 MHz, Fig. 10(b) for 900 MHz and Fig. 10(c) for 1200 MHz operation. The 2nd- and 3rd-harmonic notches move across frequency to support the various fundamental frequencies in the fixed pass-band. As shown in Fig. 10, the absolute maximum gain occurs at a frequency lower than the frequency of operation. This is a device-dependent phenomenon also observed by others (e.g., [11]) and not a product of the matching network.

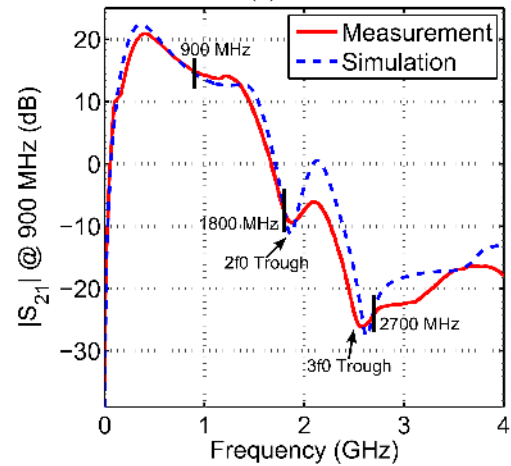
Large-signal characterization was performed using an Agilent E4438C vector signal generator to generate a continuous wave (CW) input and an Agilent E4418B power meter at the output for power measurements. The measured (simulated) power added efficiency (PAE) with the PA configured to operate at 700 MHz, 900 MHz, and 1200 MHz is 48.3% (49%), 45.1% (47%), and 30% (49%), respectively, as shown in Fig. 11(a-c). The relatively large drop in PAE at 1200 MHz is attributed to the shift in the location of the 3rd-harmonic termination seen in the small-signal response and will be discussed in more detail later.

The measured (simulated) power gain are also shown in Fig. 11(a-c) to be 16.5 dB (17.2 dB), 16.1 dB (16.1 dB), and 14.9 dB (15.6 dB) at 700 MHz, 900 MHz, and 1200 MHz, respectively. They are relatively flat up to the compression point for each mode. Finally, the measured (simulated) maximum saturated output power for each mode is 24.6 dBm (26.5 dBm), 24.0 dBm (26.0 dBm), and 20.1 dBm (25.0 dBm).

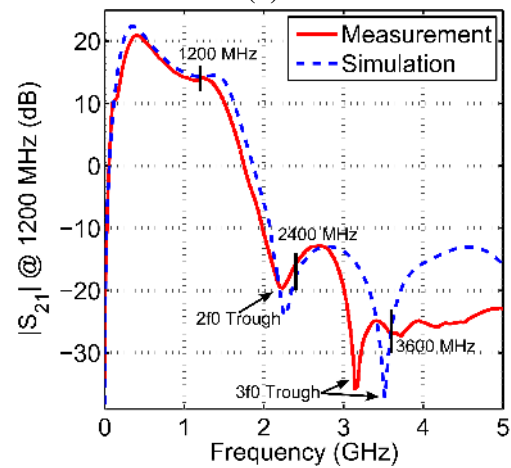
In general, there is good agreement between measurements and simulation, especially at 700 MHz and 900 MHz. There is, however, a downward shift in the location of the 3rd-harmonic notch when the PA was tuned to operate at 1200 MHz. This has



(a)



(b)



(c)

Fig. 10. Simulated and measured small signal gain at (a) 700 MHz, (b) 900 MHz, and (c) 1200 MHz.

been investigated and the shift in frequencies is due to component variation, specifically, variation in the transformer. The high-frequency mode of operation is more sensitive to component variation than the low-frequency modes, which is partially indicated by Fig. 3. In addition, increased temperature also served as a source of discrepancy in both small- and large-signal performance, specifically in the saturated output power measurements (where heating is most likely to occur).

Our hypothesis was tested in simulation. First, the self-

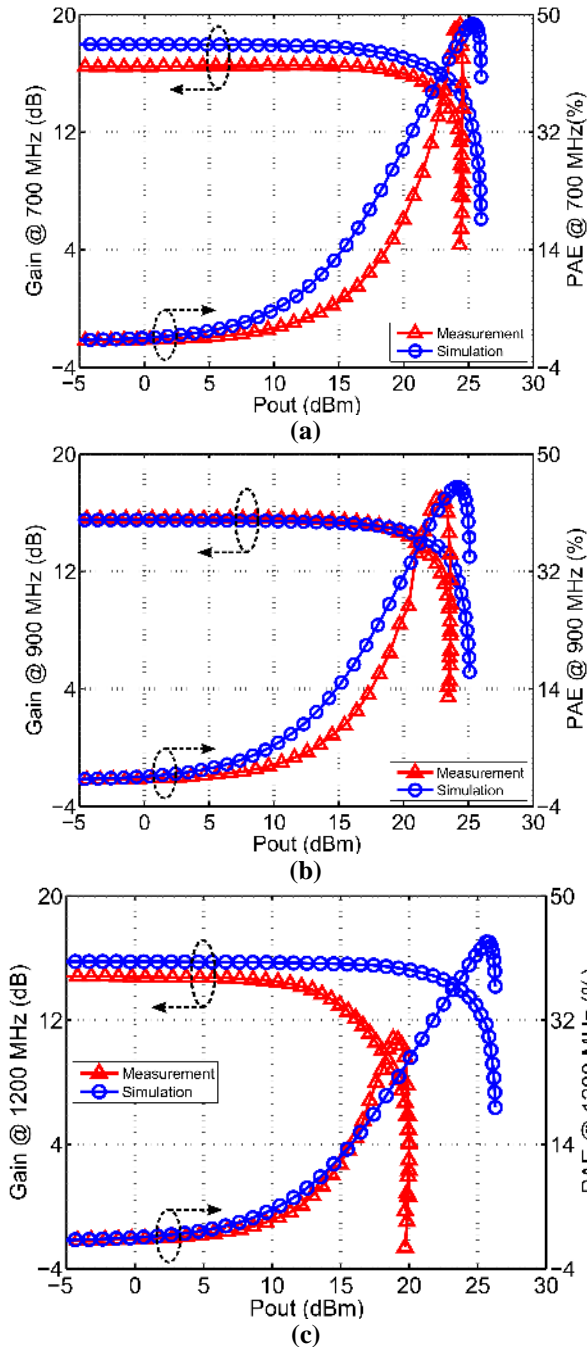


Fig. 11. Simulated and measured large signal gain and PAE at (a) 700 MHz, (b) 900 MHz, and (c) 1200 MHz.

inductance of L_{2f_0} was increased from 1.74 nH to 1.95 nH and L_2 was increased from 1.9 nH to 2.12 nH, a change of 1.2% and 12%, respectively. In addition, the part temperature was increased in simulation which brought the measurement and simulation values into close agreement as shown in Fig. 12. We also compared measurement results at 700 and 900 MHz to simulation using these new values for L_{2f_0} and L_2 in Fig. 13 and Fig. 14. It can be seen that there is still good agreement between measurements and simulation supporting our hypothesis. Table IV summarizes the measured results and compares them with previously published works (both tunable PAs and non-). It is seen that the proposed PA has among the highest PAE and saturated output power of all fully-integrated

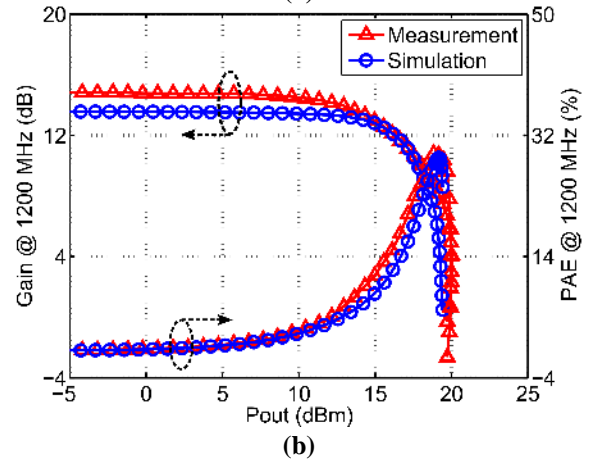
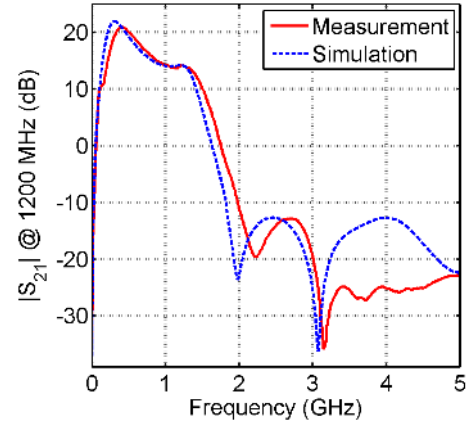


Fig. 12. Simulated and measured (a) small-signal gain and (b) large-signal gain and PAE for 1200 MHz using after model correction.

CMOS PAs. In addition, this design provides a significant tuning range thus supporting a wide range of carrier frequencies. The relatively high output power achieved in [1] can be attributed to the use of off-chip components, including transmission lines, for the matching network which provide higher Q.

V. CONCLUSION

A novel transformer-based 700–1200 MHz class-F PA with real-time tunable harmonic termination capability is proposed and fabricated in a standard 0.13 μm CMOS process. A stacked-FET approach is used for the core device in order to overcome the low breakdown voltage common with CMOS processes. This, in turn, allows the use of a higher supply voltage for higher output power and high efficiency. The fabricated PA exhibits a maximum measured PAE of 48.3%, 45.1%, and 30% for operation at 700 MHz, 900 MHz, and 1200 MHz, respectively, with a saturated output power ranging from 20.1 to 24.6 dBm. We have demonstrated that the proposed reconfigurable harmonic matching network provides a means for achieving high output power and efficiency over a wide range of operating frequencies vital for the next generation cognitive wireless communication systems.

ACKNOWLEDGMENT

The authors would like to thank MOSIS, Marina del Rey,

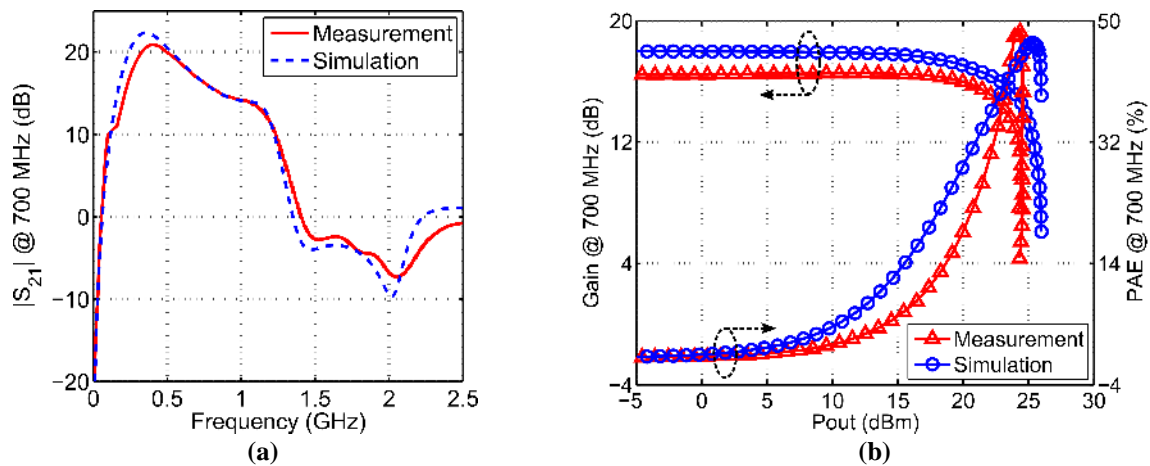


Fig. 13. Simulated and measured (a) small-signal gain and (b) large-signal gain and PAE for 700 MHz using the corrected model.

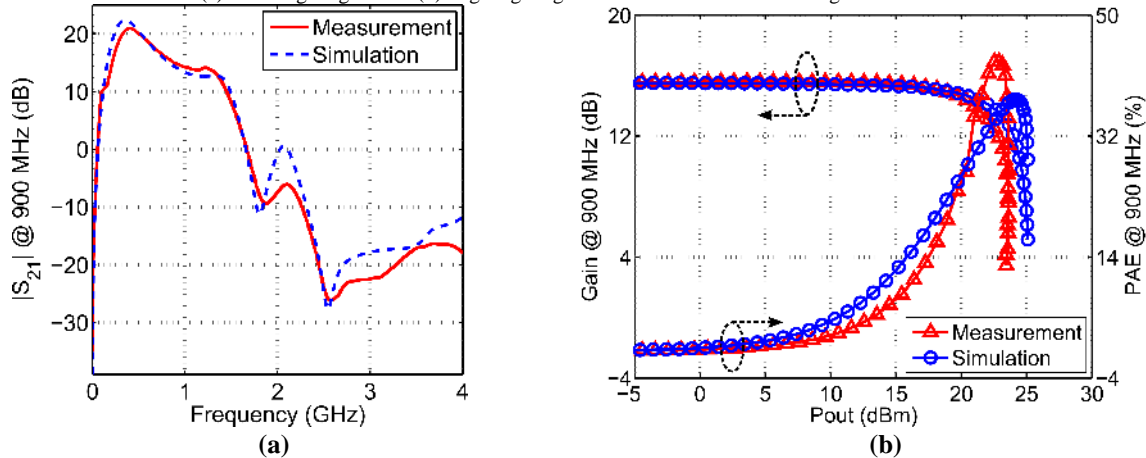


Fig. 14. Simulated and measured (a) small-signal gain and (b) large-signal gain and PAE for 900 MHz using the corrected model.

CA, for providing fabrication support.

REFERENCES

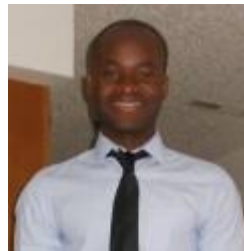
- [1] S. Pornpromlikit, J. Jeong, C. D. Presti, A. Scuderi, and P. M. Asbeck, "A watt-level stacked-FET linear power amplifier in silicon-on-insulator CMOS," *IEEE Trans. on Microw. Theory Techn.*, pp. 57-64, vol. 58, Jan. 2010.
- [2] H. Pin-Cheng, T. Zuo-Min, L. Kun-You, and W. Huei, "A high-efficiency, broadband CMOS power amplifier for cognitive radio applications," *IEEE Trans. on Microw. Theory Techn.*, pp. 3556-3565, vol. 58, Dec. 2010.
- [3] W. Hua, C. Sideris, and A. Hajimiri, "A CMOS broadband power amplifier with a transformer-based high-order output matching network," *IEEE J. Solid-State Circuits*, pp. 2709-2722, vol. 45, Dec. 2010.
- [4] V. Carrubba, J. Lees, J. Benedikt, P. J. Tasker, and S. C. Cripps, "A novel highly efficient broadband continuous class-F RFLPA delivering 74% average efficiency for an octave bandwidth," *IEEE MTT-S Int. Microwave Symp. Dig.*, pp. 1-4, 2011.
- [5] J. Taehwan, K. Bonhoon, and H. Songcheol, "A WLAN RF CMOS PA with large-signal MGTR method," *IEEE Trans. Microw. Theory Techn.*, pp. 1272-1279, vol. 61, Mar. 2013.
- [6] C. Yunsung, K. Daehyun, K. Joosung, K. Dongsu, P. Byungjoon, and K. Bumman, "A dual power-mode multi-band power amplifier with envelope tracking for handset applications," *IEEE Trans. Microw. Theory Techn.*, pp. 1608-1619, vol. 61, Apr. 2013.
- [7] Z. Chunna and A. E. Fathy, "A novel reconfigurable power amplifier structure for multi-band and multi-mode portable wireless applications using a reconfigurable die and a switchable output matching network," *IEEE MTT-S Int. Microwave Symp. Dig.*, pp. 913-916, 2009.
- [8] Q. Dongjiang, R. Molfino, S. M. Lardizabal, B. Pillans, P. M. Asbeck, and G. Jerinic, "An intelligently controlled RF power amplifier with a reconfigurable MEMS-varactor tuner," *IEEE Trans. Microw. Theory Techn.*, pp. 1089-1095, vol. 53, Mar. 2005.
- [9] Z. Haitao, G. Huai, and L. Guann-Pyng, "Broad-band power amplifier with a novel tunable output matching network," *IEEE Trans. Microw. Theory Techn.*, pp. 3606-3614, vol. 53, Nov. 2005.
- [10] Z. Xing, L. Roy, and R. E. Amaya, "1 W, highly efficient, ultra-broadband non-uniform distributed power amplifier in GaN," *IEEE Microw. Compon. Lett.*, pp. 208-210, vol. 23, Apr. 2013.
- [11] F. Fortes and M. J. Rosario, "Second harmonic class-F power amplifier in standard CMOS technology," *IEEE Trans. Microw. Theory Techn.*, vol. 49, pp. 1216-1220, Jun. 2001.
- [12] H.-Y. Liao, J.-H. Chen, H.-K. Chiou, and S.-M. Wang, "Harmonic control network for 2.6 GHz CMOS class-F power amplifier," *IEEE Int. Symp. Circuits and Systems*, pp. 1321-1324, 2009.
- [13] Yun Yin, B. Chi, and Z. Wang, "A 0.1-1.5 GHz dual-mode class-AB/class-F power amplifier in 65nm CMOS," *IEEE Midwest Symp. Circuits and Systems*, pp. 372-375, 2013.
- [14] B. Koo, T. Joo, Y. Na, and S. Hong, "A fully integrated dual mode CMOS power amplifier for WCDMA applications," *IEEE Solid-State Circuits Conf.*, pp. 82-84, 2012.
- [15] P. Wright, J. Lees, P. J. Tasker, J. Benedikt, and S. C. Cripps, "An efficient, linear, broadband class-J-mode PA realized using RF waveform engineering," *IEEE Int. Microwave Symp.*, pp. 653-656, Jun. 2009.
- [16] N. M. Neihart, A. El-Gouhary, Y. Li, K. Sessou, and X. Yu, "Techniques for realizing reconfigurable RF building blocks for cognitive radio," *IEEE Int. Midwest Symp. on Circuits and Systems*, pp. 876-879, Aug. 2013.
- [17] X. Yu and N. M. Neihart, "Analysis and design of a reconfigurable multimode low-noise amplifier utilizing a multitap transformer," *IEEE Trans. on Microw. Theory Techn.*, vol. 61, pp. 1236-1246, Mar. 2013.
- [18] N. M. Neihart, J. Brown, and X. Yu, "A dual-band 2.45/6 GHz CMOS LNA utilizing a dual-resonant transformer-based matching network," *IEEE Trans. Circuits Syst. I, Reg. Papers*, vol. 59, no. 8, pp. 1743-1751, Aug. 2012.

TABLE IV. SUMMARY OF POWER AMPLIFIER PERFORMANCE COMPARED TO PREVIOUSLY PUBLISHED DESIGNS

Reference	Technology	Frequency (GHz)	Modulation Scheme	Max VDD (V)	P _{sat} (dBm)	Peak PAE (%)	Max Gain (dB)	Area (mm ²)	Class	Notes
[1]	0.13 μm SOI CMOS	1.9	WCDMA	6.5	29.4	41.4	14.6	0.671	AB	OMN with off-chip stubs
[2]	0.18 μm CMOS	1–5	64 QAM 54 Mb/s	5.0	20–22	18–36	18–20	0.684	N/A	series transformers on-chip at input
[3]	90 nm CMOS	5.2–13	CW	2.8	25.2	21.6	18.5	0.698	AB	Fully integrated
[22]	0.13 μm CMOS	0.6–2.8	CW	1.5	21	16 (drain)	20	3.60	A	Fully integrated
[23]	0.18 μm CMOS	5.0	CW	2.0	15.4	40.6	NA	0.810	E	Fully integrated
[5]	0.13 μm CMOS	2.4	64 QAM 54 Mb/s	3.3	19.5	24.8	21	1.12	B/C	Fully integrated
[24]	65 nm CMOS	1.8	CW	3.3	18.0	21.3	12.5*	5.2	G	Fully integrated
[25]	0.18 μm CMOS	1.95	CW	3.4	26.0	46.4	26	0.832	N/A	Fully integrated
[26]	90 nm CMOS	1.9	CW	2.5	24.0	12	NA	3.69	E	Fully integrated
[27]	0.18 μm CMOS	1.95	WCDMA	3.3	26.0	20	19.9	1.32	N/A	Two chip with LINC**
[11]	0.6 μm CMOS	1.9	CW	3.0	22.8	42	10.5	N/A	F	MMIC
[12]	0.18 μm CMOS	2.6	WiMAX	1.8	20.2	24.4	13.1	0.998	F	Off chip Harmonic Control
[13]	65 nm CMOS	0.1–1.5	CW	2.5	24.2	64.0	23	N/A	AB/F	Off chip Harmonic control
[28]	0.18 μm CMOS	0.824–0.915	3G LTE	3.3	26.7	32.2	31.2	1.496	F	Off chip OMN and feedback
[14]	0.18 μm CMOS	1.95	CW	3.4	30.5	42.1	24	2.727	N/A	Fully integrated
[29]	0.25 μm CMOS SOS	1.4	CW/LTE /WCDMA	16	34.4	38	11	2.16	N/A	Off chip Choke
This Work	0.13 μm CMOS	0.7–1.2	CW	4.8	24.6–20.1	48.3–30.0	16.5–14.9	2.25	F	Fully integrated

* Drain Efficiency ** Linear amplification using nonlinear components

- [19] A. Grebennikov, N. O. Sokal, and M. J. Franco, *Switchmode RF and Microwave Power Amplifiers*, Second ed.: Academic Press, 2012.
- [20] Y. Itoh, M. Nii, Y. Kohno, M. Mochizuki, and T. Takagi, "A 4 to 25 GHz 0.5 W monolithic lossy match amplifier," *IEEE MTT-S Int. Microwave Symp. Dig.*, pp. 257–260, 1994.
- [21] S. C. Cripps, *Advanced Techniques in RF Power Amplifier Design*, First ed. Norwood, MA, Artech House, Inc., 2002
- [22] J. Roderick and H. Hashemi, "A 0.13 μm CMOS power amplifier with ultra-wide instantaneous bandwidth for imaging applications," *IEEE Int. Solid-State Circuits Conf.*, pp. 374–375, 375a, 2009.
- [23] Y. Yamashita, D. Kanemoto, H. Kanaya, R. K. Pokharel, and K. Yoshida, "A CMOS class-E power amplifier of 40 % PAE at 5 GHz for constant envelope modulation system," *IEEE 13th Topical Meeting on Silicon Monolithic Integrated Circuits in RF Systems*, pp. 66–68, 2013.
- [24] K. Onizuka, S. Saigusa, and S. Otaka, "A 1.8GHz linear CMOS power amplifier with supply-path switching scheme for WCDMA/LTE applications," *IEEE Int. Solid-State Circuits Conf.*, pp. 90–91, 2013.
- [25] H. Jeon, O. Lee, K. H. An, Y. Yoon, H. Kim, K. W. Kobayashi, C. H. Lee, and J. S. Kenney, "A cascode feedback bias technique for linear CMOS power amplifiers in a multistage cascode topology," *IEEE Trans. Microw. Theory Techn.*, pp. 890–901, vol. 61, Feb. 2013.
- [26] V. Bhagavatula, W. C. Wesson, S. K. Shin, and J. C. Rudell, "A fully integrated, regulatorless CMOS power amplifier for long-range wireless sensor communication," *IEEE J. Solid-State Circuits*, pp. 1225–1236, vol. 48, May 2013.
- [27] L. Hongtak, L. Hyun-Yong, P. Ji-Seon, and H. Songcheol, "A CMOS power amplifier for multi-mode LINC architecture," *IEEE Radio and Wireless Symp.*, pp. 41–44, 2010.
- [28] J. H. Kim and C. S. Park, "A feedback technique to compensate for AM-PM distortion in linear CMOS class-F power amplifier," *IEEE Microw. Compon. Lett.*, vol. 24, pp. 725–727, Jul. 2014.
- [29] J. Chen, S. R. Helmi, D. Nobbe and S. Mohammadi, "A fully-integrated high power wideband power amplifier in 0.25 μm CMOS SOS technology," *IEEE Int. Microwave Symp.*, pp. 1–3 Jun. 2013.



Kossi K. Sessou (S'11—M'14) received the B.S. and M.S. degrees in electrical and computer engineering from Iowa State University, Ames, in 2012 and 2014, respectively. In 2012 he joined Skyworks Solutions, Inc., Cedar Rapids, as an engineering co-op, where he was involved in power amplifier design for LTE applications. In 2013, Kossi joined MoSys Inc., Ames, as an analog and mixed signal design engineer.



Nathan M. Neihart (M'09—SM'14) received both the B.S. and M.S. degrees in Electrical and Computer Engineering from the University of Utah, Salt Lake City, in 2004. He received the Ph.D. degree in Electrical Engineering from the University of Washington, Seattle, in 2008, where he received the Analog Devices Inc., Outstanding Student Designer Award in 2007. In 2008 he joined Iowa State University, Ames, where he is now an Associate Professor of Electrical and Computer Engineering. His research interests include reconfigurable RF circuits and systems for multi-band/multi-mode radios and

circuits and systems for sensing applications. From 2010 to 2012, Dr. Neihart served as an Associate Editor for the IEEE Transactions on Circuits and Systems-II: Express Briefs and from 2012 to 2014, as an Associate Editor for the IEEE Transactions on Circuits and Systems-I: Regular Papers